α-Synuclein as a Target for Metallo-anti-neurodegenerative Agents

Kaiming Cao,[a]† Yang Zhu,[a]† Manman Liu,[a] Yanyan Yang,[a] Hongze Hu,[a] Yi Dai,[a] Yu Wang,[a] Siming Yuan,[a] Jiaming Mei,*[a] Peter J. Sadler,*[b] and Yangzhong Liu*[a]

[a] Dr. K. Cao, Dr. Y Zhu, Dr. M Liu, Mrs. Y Yang, Dr. H Hu, Prof. Y Dai, Dr. Y Wang, Dr. S Yuan, Dr. J Mei, Prof. Y Liu
Department of Chemistry; Department of Neurosurgery, Department of Pharmacy, the First Affiliated Hospital of USTC, Division of Life Sciences and Medicine, University of Science and Technology of China
Hefei, 230026 China
E-mail: liuyz@ustc.edu.cn; doctormeijiaming@163.com

[b] Prof. P.J. Sadler
Department of Chemistry, University of Warwick,
Coventry, CV4 7AL UK
E-mail: P.J.Sadler@warwick.ac.uk;

[†] These authors contributed equally to this work.

Supporting information for this article is given via a link at the end of the document.

Abstract: The unique thermodynamic and kinetic coordination chemistry of ruthenium allows it to modulate key adverse aggregation and membrane interactions of the abundant brain protein α-synuclein (α-syn). α-Syn regulates synaptic vesicle trafficking and neurotransmitter release, and is implicated in Parkinson's, a neurodegenerative disease. We show that the low-toxic octahedral Ru(III) complex *trans*-[ImH][$RuCl_4(Me_2SO)(Im)$] (NAMI-A) has dual inhibitory effects on both aggregation and membrane interactions of α-syn, and disassembles pre-formed fibrils. NAMI-A abolishes the cytotoxicity of α-syn towards neuronal cells and mitigates neurodegeneration and motor impairments in a rat model of Parkinson's. Multinuclear NMR and MS analyses show that NAMI-A binds to residues involved in protein aggregation and membrane binding. NMR studies reveal the key steps in pro-drug activation for the protein interactions. This work provides insight into the NAMI-A reaction and the effect on protein folding, and suggests a new strategy for designing ruthenium complexes which could mitigate α-syn-induced Parkinson's pathology differently from organic agents.

Introduction

Metallodrugs, such as cisplatin, offer unique medicinal properties because of their wide variety of oxidation states, coordination numbers and geometries, together with a wide range of ligand substitution rates and redox potentials.[1] Metal complexes can occupy chemical space and control the dynamics of biological reactions in quite different ways to organic compounds. Within the transition (d-block) metals, the first row elements usually have relatively high ligand substitution rates, whereas the third row metal complexes are usually more inert. We consider here the second-row $4d^5$ metal ion Ru(III) and its intriguing intermediate behavior, forming stable complexes and yet with low activation energies for ligand exchange, which allow them to reach biological target sites as pro-drugs and then undergo controlled activation.

The potential for clinical use of ruthenium is already apparent. Two complexes *trans*-[ImH][$RuCl_4(Me_2SO)(Im)$] (Im = imidazole; NAMI-A) and Na[*trans*-$RuCl_4(Ind)_2$] (Ind = indazole; KP1019) have been on clinical trials as anticancer agents, though have not achieved sufficient efficacy to be approved as new drugs.[2] The low toxicity of NAMI-A in clinical patients was notable.[3] In addition the relatively inert octahedral *tris*-diimine Ru(II) complex TLD1433 is showing promising results in photodynamic therapy for bladder cancer.[4]

Proteins appear to be targets for biologically active Ru(III) complexes.[5] The reactivity of Ru(III) complexes towards proteins have been confirmed for several model proteins, although their significance in the biological activity is not clear.[6] The molecular mechanism of NAMI-A on anti-metastasis is largely unknown.[7] Several proteins have been found to be associated with the function of NAMI-A;[6] however, it is unclear whether these proteins are the direct binding targets, and how NAMI-A reaction affects the folding and functions of proteins. Recently we proposed that the anti-metastatic activity of NAMI-A may involve interactions with the DNA-binding zinc finger transcription factor protein Sp1.[8] Here we study interactions of NAMI-A with the abundant brain protein α-synuclein (α-syn).

It is estimated that more than 50 million people in the world suffer from neurodegenerative diseases, the most common being Alzheimer's and Parkinson's.[9] Currently there is no treatment that slows disease progression and no known cure. New treatments are urgently needed. The self-assembly and aggregation of α-syn in dopaminergic neurons are thought to be closely associated with the pathogenesis Parkinson's disease (PD).[10] Thus, targeting α-syn and suppression of its aggregation is a potential therapeutic strategy.[11] However, the disordered nature of the protein hampers structure-based drug design of inhibitors of α-syn aggregation in the Lewy bodies (LBs). Moreover, the mechanism of α-syn aggregation is complicated and highly dependent on environmental

conditions, such as pH, temperature, and contact with surfaces.[12] Therefore, it is highly challenging to design rationally inhibitors of α-syn aggregation and the associated toxicity.

Membrane binding is another pathological mechanism of α-syn-associated PD.[13] The binding of α-syn to lipid membranes imparts partial helical character to the monomer.[14] This primary nucleation step accelerates fibril formation.[15] The inhibition of lipid interaction has recently been shown to be a promising approach for inhibiting the pathological effects of α-syn, examples being the natural products squalamine and trodusquemine.[16] This lipid-centered hypothesis suggests that α-syn binding to vesicular membranes influences oligomerization and controls the pathological aggregation. Thus the interruption of lipid interactions might lead to therapeutic effects on Parkinson's disease. [17]

Abnormalities of metal metabolism in the brain are gaining increasing attention for their possible relationship to neurodegenerative diseases, for example reactive forms of iron and copper in Parkinson's and Alzheimer's brains have recently been discovered.[18] Thus the use of ruthenium, the second-row transition metal congener of first-row iron in anti-neurodegenerative agents is worthy of exploration. Iron(III) chemistry differs from that of Ru(III), which has a ca. 19% larger radius, strongly prefers octahedral over tetrahedral coordination, and low-spin over high-spin states. Both ions have a strong affinity for O, N and S amino acid side-chain ligands including Asp,Glu/His/Met,Cys, but ligand exchange on Ru(III) is slower than for Fe(III), and its redox potentials are lower. These unique properties of Ru(III) offer scope for unusual protein interactions and for the design of new medicines.

We have studied the effect of NAMI-A on the membrane binding and aggregation of α-syn, as well as on α-syn-mediated cytotoxicity towards neuroblastoma cells. The activity of NAMI-A for the treatment of PD has been verified in PD-bearing rats (Scheme 1). Also we have elucidated the mechanism of activation of the pro-drug NAMI-A, and the roles of its ligands in binding to α-syn at specific protein sites by a combination of ^{1}H, ^{13}C and ^{15}N NMR studies using ^{13}C- and ^{15}N-labelled proteins, and by mass spectrometry. These data provide a molecular basis for understanding the anti-neurodegenerative activity of NAMI-A and a new strategy for the design of anti-neurodegenerative drugs.

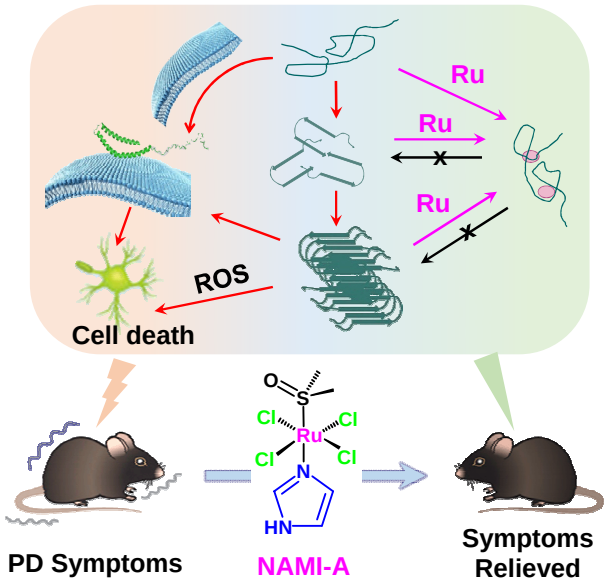

Scheme 1. Schematic illustration of the inhibition of aggregation and membrane interactions of α-syn by NAMI-A and the related therapeutic effect in the PD rat model.

Results and Discussion

NAMI-A binds to critical regions of α-syn

First, we showed that NAMI-A binds to critical regions of α-syn involved in the aggregation and fibrillation of the protein. Incubation of α-syn with NAMI-A quenched the intrinsic tyrosine fluorescence of the protein in a concentration-dependent manner (Figure S1A, S1B). The quenching was relatively rapid, half-life ($t_{1/2}$) of 10 min (Figure S1C). This timescale is consistent with the rate of ligand substitution reactions for this Ru(III) complex, i.e. substitution of NAMI-A ligands and binding of Ru(III) to the protein. [19]

ESI-MS analysis showed that the reaction of α-syn with NAMI-A led to two types of major products. The mass increases of 166.9 Da and 334.1 Da correspond to addition of one and two $[Ru(Im)]^{3+}$ fragments, respectively, to the protein (Figure 1C and Table S1). This indicates the release of chlorido and DMSO ligands from NAMI-A on coordination to α-syn. The binding of one or two $[Ru(Im)(H_2O)]^{3+}$ fragments was also observed (Figure 1D). The Ru binding sites on α-syn were further analyzed using ESI-MS with bottom-up approach. In 28 peptides obtained after enzymatic digestion, and Ru-bound peptides were detected for amino acid sequences 44-58, 98-140, 103-140 of α-syn (Figure S1D). Using these peptides as precursor ions for high energy collision-dissociation (HCD) experiments, tandem MS was applied and the Ru binding sites were narrowed down to the regions between ^{46}EGVVH^{50} and ^{114}EDMPVDPDNEAYEM^{127} by computational analysis of the peptides containing Ru fragments (software: Thermo Proteome

Discoverer). The presence of other binding sites that are not identified by this approach, such as N-terminal residues, cannot be ruled out.

The interaction between NAMI-A and α-syn in solution was studied by ^{1}H, ^{13}C and ^{15}N NMR using ^{13}C and ^{15}N-isotopically-labeled proteins (0.2 mM α-syn, 8 mol equiv Ru, 20 mM phosphate buffer, pH 7.4, 100 mM NaCl, 298 K). ^{1}H-^{15}N HSQC NMR spectra were acquired on ^{15}N isotopically-labeled α-syn (Figure 1E). Ru(III) (low-spin $4d^5$) is paramagnetic with one unpaired electron, and expected to cause broadening of peaks from nuclei in the vicinity of its binding sites. However, restricted movement of nuclei can also cause peak broadening. The differential broadening of peaks is evident in Figure 1F, 1G, S2, and S3. The plot of peak intensity attenuation throughout the amino acid sequence suggests that the binding of NAMI-A to α-syn mainly influences residues in four regions: the N-terminus, E46-A53 in the preNAC region, A69-G73 in the NACore, and E110-E131 near the C-terminus (Figure S4). The ^{1}H NMR methyl singlets of the four methionine residues decreased in intensity on reaction with NAMI-A, while many other peaks were much less affected (Figure S1E). Also in the 2D ^{1}H-^{13}C HSQC NMR spectra for selectively labeled ^{13}C-Met α-syn (Figure S1F), the methyl cross-peaks (assigned by site-mutation, see Figure S5) significantly decreased in intensity on reaction with NAMI-A. The broadening effects on His and Met of α-syn NMR peaks were similar to those we observed for reactions of NAMI-A with model amino acid derivatives (*vide infra*, Figure S6), confirming Ru(III) coordination to the Met and His residues in α-syn (Figure S7).

The NACore central region, residues 61-95, is hydrophobic and aggregation-prone, and necessary for the toxicity of α-syn; while the preNAC region (residues 47-56) is an important modulator of α-syn aggregation.[20] On the other hand, long-range interactions between the N- and C-termini of α-syn are crucial for fibril formation. The NMR data indicate that the residues of α-syn which bind to NAMI-A are all in regions involved in the aggregation of α-syn. Importantly, within these specific regions, residues M5, H50, and M127 possess high binding affinity towards Ru(III). Together with the ESI-MS data, it can be hypothesized that the binding of NAMI-A to residues that are involved in the aggregation of α-syn, plays a key role in inhibiting fibrillation and the toxicity of α-syn.

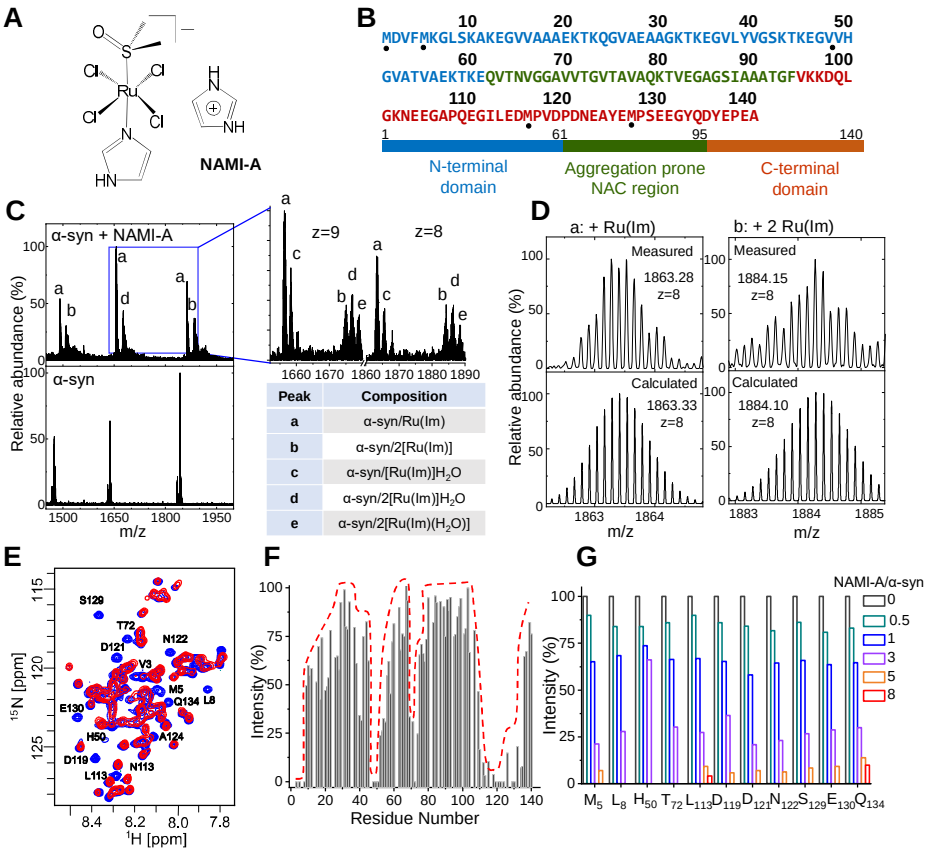

Figure 1. NAMI-A, α-syn, and NMR and MS studies of reactions. (A) Structure of NAMI-A. (B) Amino acid sequence and functional domains of α-syn. N-terminal lipid-binding domain, non-amyloid-β component (NAC) region of aggregation-prone hydrophobic domain, and C-terminal acidic-residue-rich domain.[11b] Preferential binding residues for NAMI-A are highlighted with black dots. (C) ESI-MS spectra of the Ru-bound adducts (a - e). The adduct compositions are listed underneath the spectrum. The reaction was performed on 10 μM protein and 50 μM NAMI-A at 37 °C for 2 h in 50 mM NH_4Ac. (D) The +8 charged peaks of the adducts and their theoretical isotopic patterns. (E) Superposition of ^{1}H-^{15}N HSQC NMR spectra of α-syn (0.2 mM, 20 mM phosphate buffer, pH 7.4, 100 mM NaCl, 298 K) before (blue) and after (red) reaction with NAMI-A (8 eq., 2 h). (F) The peak intensity (integral) change along the amino acid sequence of α-syn after reaction with NAMI-A determined from the NMR spectra in Figure E. (G) Intensities of 11 most affected peaks at various [NAMI-A]/[Protein] ratios based on integration of 2D HSQC cross-peaks.

Mechanism of NAMI-A interactions

To understand the nature of Ru(III) coordination to α-syn in more detail, reactions of NAMI-A with model compounds, N-acetyl-L-methionine (AcMet) and N-acetyl-L-histidine (AcHis), were studied. The ^{1}H NMR peaks for AcHis and AcMet showed little change

during the first 40 min of incubation with NAMI-A (Figure 2A, 2B). Then these signals decreased and reached equilibrium in about 2 h (Figure 2C). This result suggested that initial hydrolysis is required to activate NAMI-A for reactions with these amino acids.

Evidence that NAMI-A is activated by hydrolysis was provided by the appearance of a new paramagnetically-shifted peaks for the DMSO ligand at -11.1 ppm, the intensity of which reached a maximum within ca. 40 min. This is consistent with the rate of displacement of a Cl- ligand by H_2O (Figure S8). However, on the other hand, the appearance of a peak for free DMSO (2.72 ppm) indicated a second stage of hydrolysis. In the meantime, the peak at -11.1 ppm decreased after 40 min and disappeared in ca. 2 h, accompanied by the appearance of free DMSO (Figure 2D). This timescale for 2-step hydrolysis is consistent with the reactivity of NAMI-A towards AcMet and AcHis, suggesting that the diaqua species $[(Ru(Im)(H_2O)_2Cl_3]^+$ plays a crucial role in reactions with these amino acids (Figure 2E).

The products from the reactions of NAMI-A with AcMet and AcHis were identified by ESI-MS as $[Ru(Im)(AcMet)(Ac)]^{2+}$ and $[Ru(Im)(AcHis)(Ac)]^{2+}$, respectively (Figure S9). These model reactions are consistent with the MS data from the reactions of NAMI-A with α-syn, for which adducts containing $[Ru(Im)(H_2O)]^{3+}$ and $[Ru(Im)]^{3+}$ fragments were detected. The release of DMSO and Cl^- ligands on reaction with the protein is again consistent with pre-activation of NAMI-A by hydrolysis.

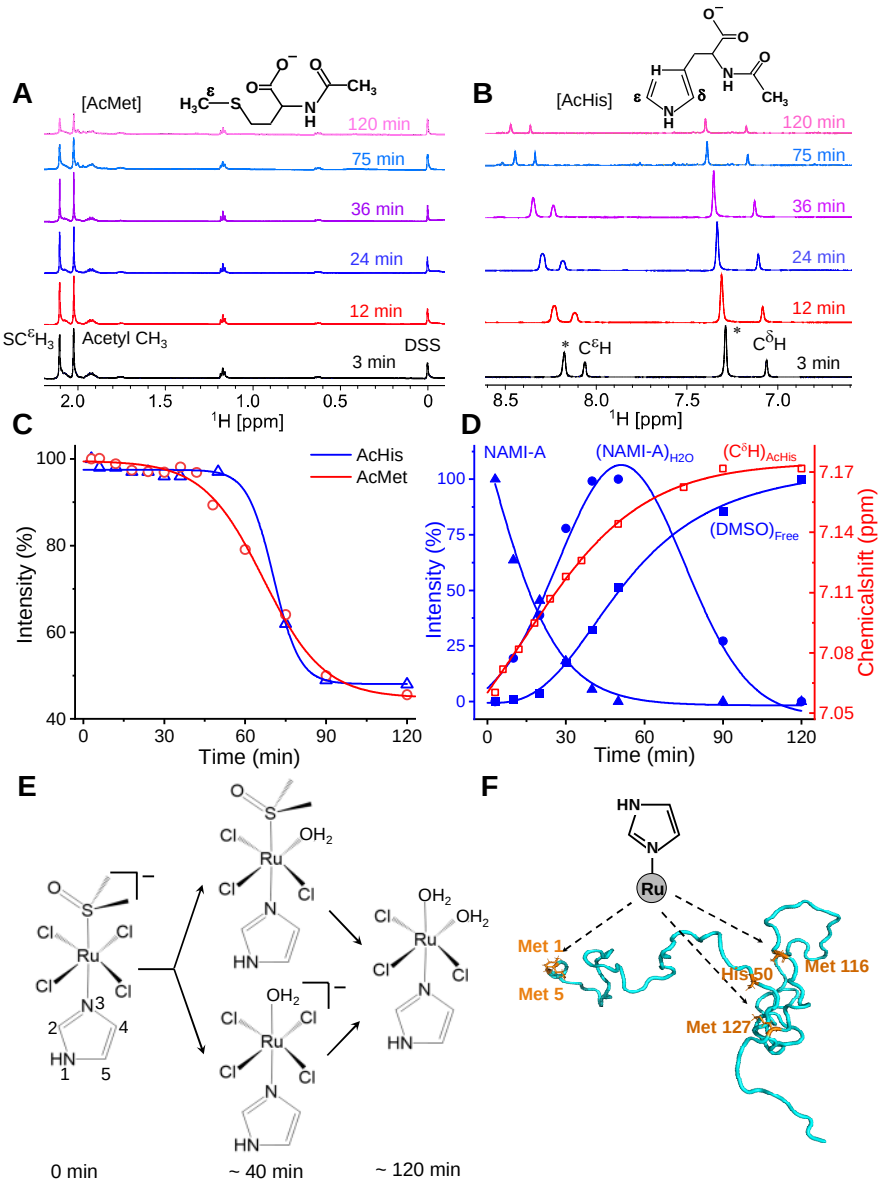

Figure 2. ^1H NMR studies of the reaction of NAMI-A with AcMet or AcHis. (A) Reaction of 1 mM AcMet with 4 mM NAMI-A after different times. Peaks of $SC^{\varepsilon}H_3$ and acetyl CH_3 of AcMet are assigned. (B) Reaction of 1 mM AcHis with 2 mM NAMI-A. Peaks of $C^{\varepsilon}H$ and $C^{\delta}H$ of AcHis are assigned. Asterisks (∗) indicate free imidazole from NAMI-A. (C) Time-dependent signal decrease (integrations) of $SC^{\varepsilon}H_3$ of AcMet and $C^{\delta}H$ peaks of AcHis in the reaction with NAMI-A. (D) Comparison of the shift of imidazole peak of AcHis $C^{\delta}H$ from (B) (red line) during the hydrolysis of free NAMI-A. NAMI-A species was based on the hydrolysis of 1 mM NAMI-A in PBS (Figure S8), including NAMI-A itself (▲), hydrolysate $(NAMI\text{-}A)_{H2O}$ (●), free DMSO after hydrolysis $(DMSO)_{Free}$ (■). (E) Pathways for NAMI-A hydrolysis based on the NMR spectra in (D). (F) Proposed interaction sites for Ru(III) on α-syn. Numbering of imidazole atoms for NAMI-A is in (E). Reactions were performed in D_2O in PBS at pH 7.4 and 310 K. DSS (0.15 mM) was used as an internal reference (0 ppm and consistent intensity) for all ^1H NMR spectra. The incubation time is labeled on each spectrum.

Besides the decrease in intensity of the imidazole ring protons of AcHis on reaction with NAMI-A, they also shifted gradually to low field. This suggested the presence of additional weaker non-covalent interactions (fast exchange on NMR timescale). Notably such a peak-shift was also observed for His50 of α-syn on reaction NAMI-A (Figure S10A and B), but not for AcMet (Figure 2A). The free imidazolium counterion from NAMI-A can also interact with the Ru(III) complex; its peaks shifted and broadened in a similar way to AcHis during the incubation (Figure S10C, D, and E). ESI-MS analysis showed the formation of a bis-imidazole adduct in the products (Figure S9E), confirming that the free imidazole from NAMI-A can react with ruthenium during the hydrolysis. Notably, the time-dependent shift of these imidazole peaks is consistent with the hydrolysis rate of NMAI-A (Figure 2D), and a similar effect on peaks was observed for His50 of α-syn.

α-Syn contains potential carboxylato and amine binding sites. ^{1}H NMR studies showed that the methyl signals ($C^{\beta}H_3$) of acetylated alanine (AcAla) decreased in area by about 17% after incubation with 4-mol equiv of NAMI-A (Figure S11A), suggesting weaker binding than AcMet (60% decrease). Ala and Lys showed similar reactivity as AcAla, suggesting minimal effects of the amino group on the reactivity of the carboxylate groups (Figure S11C). Taken together, these results indicate that NAMI-A can interact with α-syn through non-covalent binding after the hydrolysis, and then Ru(III) coordinates to the protein preferentially at His and Met residues in a relatively slow process (hours, Figure 2F). Carboxylate groups of Asp and Glu residues may also be involved in weaker binding.

NAMI-A inhibits α-syn aggregation *in vitro*

The effect of NAMI-A on the formation of α-syn amyloid fibrils was assessed using the thioflavin T (ThT) fluorescence assay. The formation of amyloid fibrils of α-syn was indicated by the increase in fluorescence of ThT. Treatment of NAMI-A with α-syn significantly reduced the florescence, implying inhibition of the fibrillation of α-syn. A time dependent ThT assay clearly showed that NAMI-A inhibition of the fibrillation of α-syn is long-lasting; little fluorescence change was observed for 64 h in the presence of NAMI-A (Figure 3A and S12).

The formation of amyloid fibrils was clearly observable for α-syn alone by transmission electron microscopy (TEM), while no fibrils were observed in the presence of NAMI-A (Figure 3B). Centrifugation of α-syn from the ThT reaction mixture resulted in precipitation of yellow ThT-containing fibrils. This was not observed for α-syn treated with NAMI-A (Figure S13). In addition, gel electrophoresis analysis confirmed that NAMI-A prevented the early oligomerization of α-syn (Figure 3C). These results clearly indicated that NAMI-A effectively inhibits the oligomerization and filamentous aggregation of α-syn. Remarkably, NAMI-A could even disassemble preformed amyloid fibrils of α-syn (Figure 3D). The ThT-assay and protein detection indicate that α-syn fibrils can form partially in 24 h and nearly completely in 48 h (Figure 3A and 3E). Adding NAMI-A to these samples disassembles the fibrils formed under both conditions in a concentration-dependent manner (Figure 3D).

Alteration of the secondary structure of α-syn during protein aggregation was studied since this typically accompanies the filamentous aggregation of proteins. Circular dichroism (CD) spectroscopic analysis showed that incubation of α-syn caused a gradual change of secondary structure from random coil to β-sheet, characterized by the reduced intensity of the negative peak at ~200 nm and increase in intensity of the negative peak at ~220 nm (Figure 3F). The presence of NAMI-A prevented the β-sheet formation. Moreover, NAMI-A could also convert the β-sheet of aggregated α-syn back to random coil (Figure 3F, red line), consistent with its ability to disassemble amyloid fibrils. It can be concluded that the protein structure necessary for the aggregation of α-syn and amyloid fibril formation is altered by NAMI-A binding.

NAMI-A suppresses membrane interactions with α-syn

In addition to protein aggregation, membrane binding is another pathological mechanism of α-syn associated Parkinson's disease.[13] The lipid-centric hypothesis suggests that α-syn binding to vesicular membranes influences oligomerization and controls the pathological aggregation, and inhibition of lipid interactions might result in therapeutic effects for Parkinson's disease.[17]

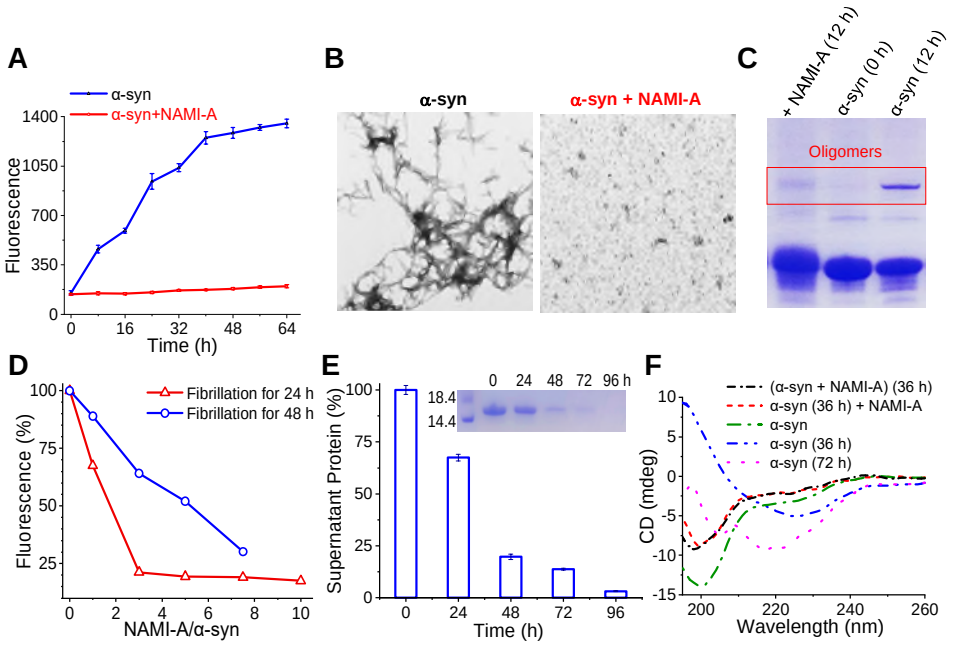

Figure 3. NAMI-A inhibits aggregation and fibrillation of α-syn. (A) ThT assay for filamentous aggregation of α-syn. α-Syn (70 μM) was incubated with ThT (20 μM), and NAMI-A (8 mol. equiv) was added at start time to evaluate the inhibition efficiency. (B) Representative TEM images of the fibrillation of α-syn in the absence (left) or presence (right) of NAMI-A. (C) SDS-PAGE analysis of the early oligomerization of α-syn and the effect of NAMI-A (8 mol. equiv). (D) Disassembly of pre-formed α-syn fibrils by NAMI-A. The fibrils were generated by the incubation of 70 μM α-syn for 24 h or 48 h, incubated with various ratios of NAMI-A for 2 h, then further incubated with ThT for 30 min before fluorescence measurements. (E) Time-dependent aggregation of α-syn during the incubation. The sample was centrifuged (18,000 g for 30 min) after incubations, and soluble α-syn in the supernatant was measured by SDS-PAGE. Some soluble aggregates may not be detected in this assay. (F) Effect of secondary structure of NAMI-A (100 μM) α-syn on the aggregation of α-syn (20 μM) studied by CD spectroscopy.

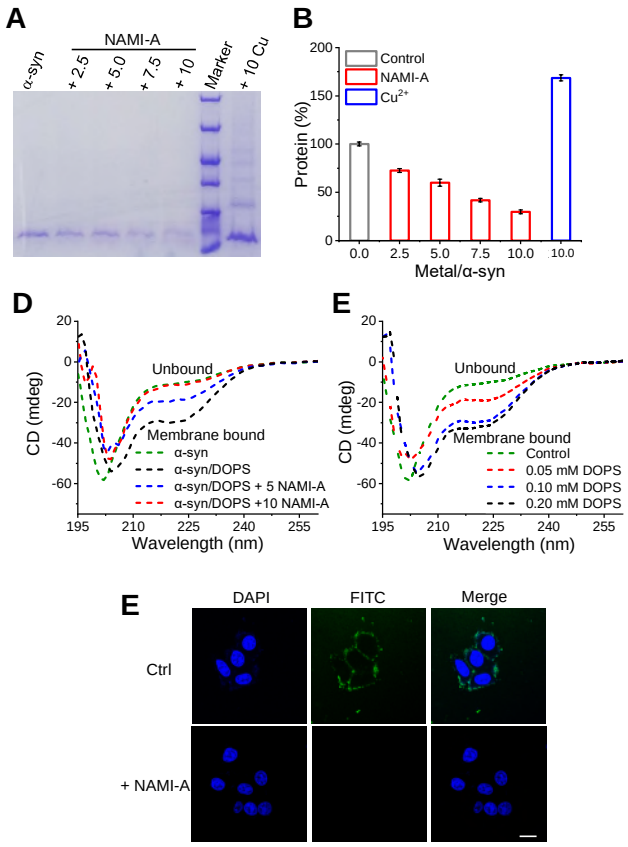

Figure 4. NAMI-A inhibits liposomal interactions of α-syn. (A-B) Lipid pull-down using 100 μM DOPS liposomes and 20 μM α-syn in the presence of various molar ratios (0, 2.5, 5, 7.5 and 10) of NAMI-A. 10 mol equiv of $CuCl_2$ was used for comparison. After 2 h of incubation, the protein in the liposomes was analyzed by gel electrophoresis. (C) Effect of membrane binding on the secondary structure of α-syn. CD spectra were recorded on 20 μM α-syn in the presence of different concentrations of DOPS in 10 mM phosphate buffer. (D) Effect of NAMI-A on interactions of α-syn with DOPS liposome membranes. CD spectra were recorded on 20 μM α-syn in the presence of 0.2 mM DOPS liposomes, and various amounts of NAMI-A (black: 0 μM; blue: 100 μM; red: 200 μM). The spectrum of α-syn alone (without DOPS and NAMI-A) was recorded for comparison (green). (E) NAMI-A inhibits the binding of α-syn to cell membranes. Confocal laser scanning microscopy images of HeLa cells pre-incubated with 10 μM FITC-labeled α-syn at 37 °C for 1 h. Then, cells were treated with 50 μM NAMI-A or PBS (Ctrl) at 37 °C for 2 h before recording the images with λ_{em} = 488 nm. (Scale bar = 20 μm)

Therefore we explored the effect of NAMI-A on the interaction of α-syn with the lipid DOPS, the most abundant phospholipid in the membranes of synaptic vesicles. After incubation of α-syn with DOPS liposomes for 30 min, the liposomes were collected by centrifugation (18000 g), and their α-syn content was determined by gel electrophoresis (Figure 4A, 4B). The presence of NAMI-A clearly reduced liposome uptake of α-syn in a dose-dependent manner. On the contrary, Cu(II) ions promoted the interaction of α-syn with the lipid (Figure 4A, 4B). Moreover, the interaction of α-syn with DOPS liposomes was observed directly by fluorescence imaging using FITC-labeled α-syn. The green fluorescence observed around liposomes clearly indicated the binding of α-syn to DOPS, while much weaker fluorescence was observed for the liposomes after NAMI-A treatment (Figure S14).

Additionally, the ability of DOPS liposome interactions to change the secondary structure of α-syn was investigated by CD spectroscopy, since the lipid interaction can induce a change in the secondary structure of α-syn from random coil to α-helix.[21] CD confirmed that the α-helical content of α-syn increased with increase in liposome concentration (Figure 4C). Addition of 10 mol equiv NAMI-A almost totally inhibited this structural change (Figure 4D). These results indicate that NAMI-A effectively inhibits membrane interactions of α-syn and the associated structural alteration to the protein.

Next, we studied the interaction of α-syn with the membranes of living cells. Confocal laser scanning microscopy images of HeLa cells treated with FITC-labeled α-syn, showed green fluorescence on the cell membrane, clearly indicating the binding of α-syn (Figure 4E). In contrast, when the cells were incubated with α-syn for 1 h and then treated with NAMI-A (50 μM, 5 mol equiv), green fluorescence from α-syn was not

observed on the cell membrane (Figure 4E). This indicates that NAMI-A can reverse cell membrane interactions of α-syn.

NAMI-A suppresses neuronal toxicity of α-syn

Since NAMI-A is capable of inhibiting both protein aggregation and membrane interaction of α-syn, the two pathological features of α-syn in PD, the effect of NAMI-A on the cytotoxicity of α-syn oligomers towards neuronal cells was investigated. Human SH-SY5Y neuroblastoma cells and PC12 phaeochromocytoma cells (neuronal model) were treated with the α-syn aggregates at (monomer) concentrations of 0.5-2 μM. The MTT assay demonstrated that α-syn oligomers inhibit the proliferation of both types of neuronal cells (Figure 5A). Pretreatment of α-syn fibrils with NAMI-A significantly reduced their cytotoxicity; SH-SY5Y and PC12 cell populations were almost unchanged when the fibrils were treated with 5 μM NAMI-A (Figure 5B, 5D). NAMI-A alone exhibited negligible effects on the proliferation of cells. In addition to eliminating the cytotoxicity of α-syn fibrils, NAMI-A can also abolish the toxicity of monomeric α-syn by inhibiting the production of toxic α-syn aggregates (Figure S15).

The generation of reactive oxygen species (ROS) in neuronal cells is reported to be associated with the neuro-toxicity of α-syn.[22] Fluorescence imaging using ROS probe 2',7'-dichlorodihydrofluorescein diacetate in SH-SY5Y cells showed that treatment with α-syn oligomers induced a sharp increase in the ROS level (Figure 5E). Upon treatment with NAMI-A, the level of cellular ROS induced by α-syn decreased significantly in a dose-dependent manner; 5 mol equiv of NAMI-A reduced the cellular ROS close to that of the control group (Figure 5E). This suggests that NAMI-A can suppress the cytotoxicity of α-syn by inhibiting the formation of intracellular ROS.

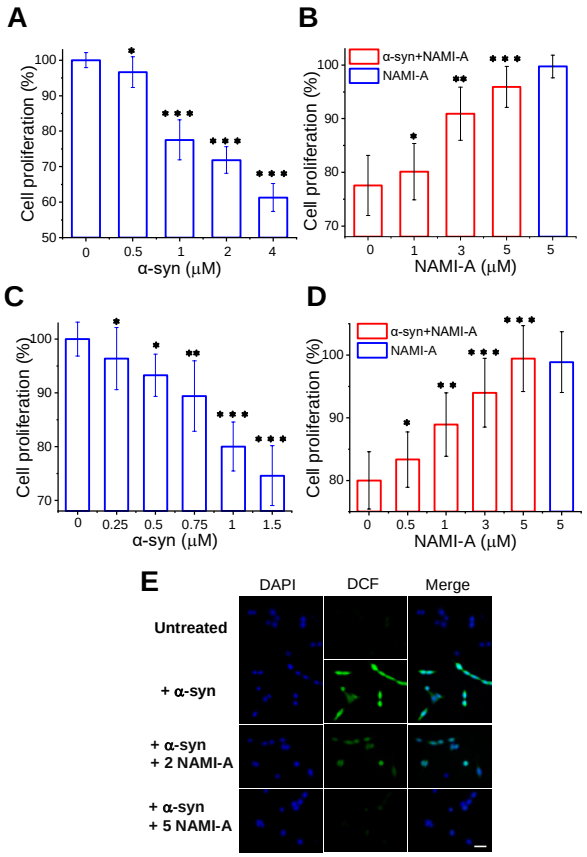

Figure 5. NAMI-A suppresses the toxicity of α-syn oligomers in human neuroblastoma cells. (A) MTT assay for the cellular viability of SH-SY5Y neuroblastoma cells, and (C) PC12 cells, after treatment with α-syn oligomers. (B) Effects of NAMI-A on α-syn oligomer-induced toxicity in SH-SY5Y cells, and (D) PC12 cells. The α-syn oligomers (1 μM) were resuspended and incubated with NAMI-A (1 μM, 3 μM, 5 μM) in cell culture medium for 1 h at 37 °C, and then added to the SH-SY5Y cells for 24 h. The toxicity of NAMI-A alone (24 h at 37 °C) was also determined. (E) Effect of NAMI-A on ROS production induced by α-syn oligomers in SH-SY5Y cells treated with on α-syn oligomer. Representative microscope images for SH-SY5Y cells treated with α-syn oligomers (1 μM) incubated with or without of NAMI-A (2 μM or 5 μM) for 1 h at 37 °C. The green fluorescence (DCF) from the ROS probe shows ROS level in cells. (Scale bar = 20 μm)

NAMI-A suppresses neurodegeneration and motor impairment *in vivo*

The *in vivo* effect of NAMI-A in a rat model of PD was evaluated using wild-type rats. The PD model was established by a single stereotaxic injection of preformed α-syn fibrils (PFFs) using a literature method.[23] The injection of PFFs to the substantia striatum induces Lewy body-like aggregates at the injection site as well as in the brain regions that are connected to the striatum. The appearance of α-syn pathology was verified by the progressive loss of dopaminergic neurons in the substantia nigra (SN) (Figure 6A). Thus, this disease model displays the two characteristic features of PD, i.e. Lewy body-like aggregates and neurodegeneration.

At 60 day post-injection of PFFs, the Lewy body-like pSyn (phosphorylated α-syn) aggregates at the nigra site of rats were assayed by immunohistochemistry. In agreement with literature,[23] the inoculation of PFFs at the striatum clearly led to the formation of α-syn-containing inclusions inside SN dopaminergic neurons (Figure 6B). Interestingly, the rats

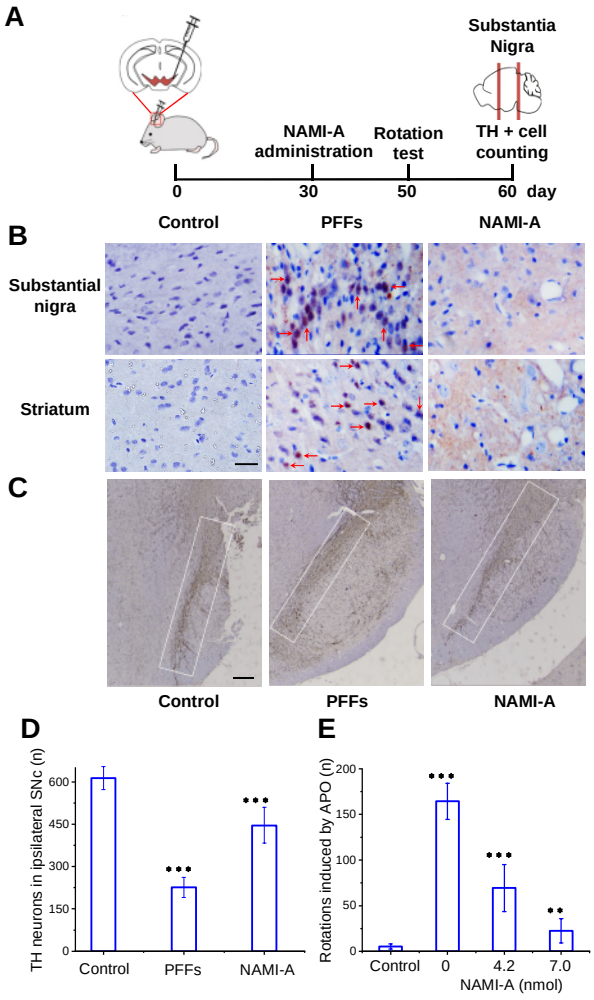

Figure 6. NAMI-A mitigates α-syn pathology, neurodegeneration, and behavioral defects in a PD rat model. (A) Schematic representation of stereotaxic injections (top portion) and experimental timeline (bottom portion). (B) Representative IHC images of pSyn in substantial nigra and striatum regions. Red arrows highlight pathology revealed by immunostaining using antibodies to pSyn (scale bar, 20 μm). (C) Representative IHC images of TH-positive neurons in the injected PFFs and the injected NAMI-A nigra regions (scale bar, 250 μm). The rats were administered 7 nmol NAMI-A on the 30th day after treatment with PFFs (1.4 nmol in monomer). (D) Quantification of TH-positive relative neuron loss in Figure B (n ≥ 4 rats). (E) PFFs-induced rotation of rats. The test was performed on the 50th day after the treatment with PFFs. Different amounts of NAMI-A (4.2 and 7 nmol) were given to the rats on the 30th day. Statistical significance: *** $p \leq 0.001$ and ** $p \leq 0.01$ significant when compared with control.

injected with NAMI-A displayed a significant reduction in α-syn pathology, as evidenced by the substantial decrease of pSyn aggregates in the nigra and striatum regions (Figure 6B). As the formation of Lewy body-like aggregates can cause neurodegeneration, we further verified the effect of NAMI-A on the recovery of neurodegeneration of the substantia nigra in rats. At 60 days post-injection, tyrosine hydroxylase (TH), the rate-limiting enzyme in dopamine synthesis, in dopaminergic neurons was analysed using immunohistochemistry (IHC). The rats injected with PFFs exhibited a considerable loss of dopaminergic neurons. In comparison,

treatment with NAMI-A resulted in marked protection of TH-positive neurons, reducing neuron loss from 63% to 27% (Figure 6C, 6D). It has been reported that the cell-to-cell spread of PFFs can occur through receptor-mediated transmission.[24] Here we found that a single intrastriatal inoculation of recombinant α-syn fibrils led to the loss of dopamine neurons in the substantia nigra pars compacta, which is consistent with the intercellular transmission of α-syn pathology. The reduced neuronal damage in the substantia nigra suggests that treatment with NAMI-A can also inhibit the spreading of α-syn between cells.

The effect of NAMI-A on motor functions in PD rats was further evaluated in an open-field test. First, to investigate the asymmetry of the dopamine circuit in the bilateral nigrostriatal circuit, a typical rotation test was performed by using apomorphine (APO), since the APO-induced rotation is a characteristic feature of PD patients. APO is an agonist, which stimulates both classes of dopamine receptors (D1, D2), and therefore directly affects presynaptic or auto receptors and postsynaptic or heteroreceptors. A challenge with intraperitoneal APO hydrochloride, 0.5 mg/kg, for 30 min, was performed at day-60 after the stereotaxic injections of preformed α-syn fibrils. Contralateral turning was readily observed. During turning, the pattern of stepping was apparently asymmetrical, that is, the forepaw ipsilateral to the lesion was found to step sideways, whereas the contralateral forepaw was stretched away and pulled along. Since the contralateral hind paw remained stationary, the rats actually turned around this paw ('pivoting'). Meanwhile, its head touched its tail, curving like a cycle rotating at a rapid speed (Figure S16). Thus, the ipsilateral forelimb appeared to determine the pattern and direction of stepping whereas the contralateral limbs were mostly akinetic. In comparison, no obvious contralateral turning was observed in the rats treated with NAMI-A (Figure 6E). These data indicate that NAMI-A can effectively rescue motor impairments induced by α-syn aggregates. Thus NAMI-A appears to inhibit the *in vivo* neurotoxicity of α-syn fibrils and protects animals against neurodegeneration and motor impairments.

DISCUSSION

α-Syn is the most abundant protein in Lewy bodies,[25] which play a major role in neurological disorders, including the development of PD through multiple cellular processes.[26] Hence, targeting the aggregation of α-syn is a promising therapeutic strategy for mitigating the pathology of the disease.[27] Because of the unstructured nature of α-syn, it is difficult to design rationally inhibitors of this aggregation, so screening large chemical libraries is generally used instead. It is known that the aggregation of α-syn can be modulated by metal ions, such as Fe(III) and Cu(II); and ion mobility-MS studies have shown that these first row transition metal ions can bind to protein regions crucial for the aggregation, and cause 'compactation' of the structure.[28] Metallodrugs may therefore offer a viable strategy for disrupting α-syn aggregation and treating the associated diseases. Complexes of the second row transition metal ion Ru(III) are more inert than those of the first row, and the ligands can play a prominent role in both delivery of the metal to target sites and its subsequent effect on protein structure.

The octahedral Ru(III) drug NAMI-A has already undergone clinical trials as an anticancer/ antimetastatic agent. Clinical trials of NAMI-A were terminated on account of a lack of efficacy,[29] but NAMI-A showed low toxicity in phase II clinical trials.[29] An x-ray crystallographic study on a model protein (hen egg-white lysozyme) indicates that NAMI-A can bind to proteins with the substitution of chlorido and DMSO ligands; while the imidazole ligand remains strongly bound to Ru(III).[30] It is unknown how these substitution processes occur, or the consequences for protein function. Here we found that NAMI-A binds to α-syn after activation steps involving hydrolysis. The uniform ^{15}N labeling and selective ^{13}C-Met labeling allowed detailed NMR studies of reactions of α-syn with NAMI-A, and the sequence-dependent influence on the protein residues. Kinetic studies revealed that, in contrast to labile metal ions, the strongly-bound bulky imidazole ligand in NAMI-A introduces steric hindrance towards attack on Ru(III), and prevents intermolecular interactions that lead to protein aggregation. Not only can NAMI-A inhibit aggregation, but more significantly, is also capable of disassembling pre-formed amyloid fibrils of α-syn. α-Syn amyloid inclusions have been observed in dopaminergic neurons of PD patients. Hence the disassembly of the amyloid is important for reversing the development and progress of PD disease. Although a variety of molecules which inhibit the aggregation of α-syn have been identified, it is still a challenge to disassemble preformed amyloid fibrils because of their high stability, and there are few reports of success.[31]

In addition to α-syn aggregation, membrane binding is another pathological mechanism associated with Parkinson's disease.[32] The membrane interaction alters the secondary structure of α-syn and promotes the aggregation; which increases the toxicity of the protein. The amino acid sequence of α-syn contains several motifs that tend to form amphipathic α-helices. These motifs mediate association of α-syn with lipid membranes, while the membrane interaction stabilizes the α-helical structure.[14] Also the hydrophobic NACore of α-syn, which is necessary for the aggregation and toxicity, can interact with membranes, and this interaction promotes the formation of α-helix in this region.[21, 33] It is believed that the membrane binding controls the pathological aggregation and toxicity of α-syn.[17a] Therefore, interference with lipid interactions can be an effective therapeutic strategy for Parkinson's disease.[16a, 34] While several inhibitors have been developed to target the fibrillation of α-syn, very few inhibitors of membrane interactions have been reported.[35] Here we found that NAMI-A has dual inhibitory effects on the α-syn associated pathology: inhibition of amyloid fibril formation as well as the interaction with the membranes of neuronal cells.

Epidemiological studies suggest that occupational and environmental exposure to metals (Mn, Cu, Fe, Zn) increase the risk of PD.[36] In addition, alterations in metal homeostasis are associated with the progression of

α-syn amyloid assembly and the onset of PD.[17b] Cu(II) ions promote helix formation by α-syn on membranes.[37] There is a high-affinity Cu(II) site near the N-terminus,[38] and Cu(II) binding to His50 accelerates α-syn aggregation, destabilizing the soluble native conformation of α-syn.[39] Labile first-row transition metal ions can readily promote aggregation by intermolecular protein cross-linking. Ru(III) possesses high binding affinity for methionine and histidine residues.[40] Here, the NMR analyses reveal that NAMI-A binding occurs in Cu(II)-binding regions of α-syn, and also in a number of other areas. Because of the differences in coordination geometries (Cu(II) being prone to distorted octahedral coordination), ligand affinities, and dynamics of ligand exchange, the nature of the conformational change in α-syn induced by interaction with Ru(III) from NAMI-A differs from that induced by Cu(II) binding. The chlorido, imidazole and DMSO ligands on octahedral Ru(III) in NAMI-A all play roles in controlling the kinetics and spatial direction of both activation (hydrolysis) and exchange with protein ligands. Reaction of α-syn with NAMI-A results in bound Ru(III) with the initial imidazole ligand still coordinated. The presence of bulky imidazole introduces steric hindrance at the ruthenium binding site, which can prevent the intermolecular interaction that leads to protein aggregation. Hence, the effects of NAMI-A on α-syn aggregation are dramatically different from those of Cu(II) and Zn(II).

Our NMR data suggest the pre-recognition of NAMI-A by α-syn involving non-covalent interactions prior to direct Ru(III) coordination. Such a mechanism has recently been described for NAMI-A binding to lysozyme: initial non-covalent binding involving H-bonds and cation-π interactions of Ru-imidazole with Arg, Lys and Asn residues, followed by release of its ligands step-by-step; and eventual Ru(III) coordination to a histidine residue of the protein.[30] These data also suggest that NAMI-A binds to α-syn at N- and C-terminal residues, as well as the NACore region. This binding could prevent the transmission of α-syn fibrillation. It has been reported that the spread of α-syn fibrils, including cell-to-cell propagation, is a common process in the progression of the disease.[41] Lymphocyte activation gene 3 (LAG3) and amyloid precursor-like protein 1 (APLP1) are receptors on the cell surface that preferentially bind to α-syn amyloid to fulfill intercellular transmission. This interaction is typically achieved by the binding of the alkaline surface of receptors to the acidic C-terminus of α-syn.[24] Targeting of the interaction between α-syn and the receptor would prevent the transmission of α-syn, and is therefore is a potential strategy for PD treatment.[24]

Due to the prominent inhibitory activity towards the pathological factors associated with α-syn, NAMI-A significantly reduces the toxicity of α-syn aggregates to neuronal cells. NAMI-A nearly completely prevents ROS production in cells induced by α-syn. Remarkably, the *in vivo* assay on rats shows that NAMI-A can effectively reverse symptoms of Parkinson's disease caused by α-syn fibrils, implying potential therapeutic potency. While a large number of agents have been reported to inhibit the aggregation of α-syn and are capable of reducing the toxicity of α-syn on cells, very few of them have been shown to be effective in mammalian PD models.[11b] This remarkable *in vivo* effect of NAMI-A is probably associated with its dual inhibition of both aggregation and membrane binding of α-syn.

Conclusion

In summary, we have identified the key steps in the activation of the octahedral Ru(III) prodrug NAMI-A in its reaction with the abundant brain protein α-syn, a potential target for treatment of neurodegenerative diseases such as Parkinson's. Moreover, we have been able to correlate ruthenium binding sites on α-syn directly with the anti-neurodegenerative activity of NAMI-A. NAMI-A has dual inhibitory effects on both α-syn-associated pathological features: the formation of amyloid fibrils and its membrane interactions (Scheme 1). Significantly, NAMI-A can disassemble the pre-formed fibrils of α-syn, and abolishes the cytotoxicity of α-syn oligomers towards neuronal cells. *In vivo* assays indicate that NAMI-A alleviates the α-syn-mediated pathology, including neurodegeneration and motor impairments, in PD rats. Mechanistic investigations reveal that NAMI-A binds to α-syn with substitution of chlorido and DMSO ligands, and the imidazole ligand on ruthenium plays a role in the initial non-covalent recognition of α-syn, and promotes the subsequent coordination steps. NMR analysis indicates that NAMI-A binding perturbs residues at the N-, C-termini and NACore, especially histidines and methionines, in regions involved in protein aggregation and membrane binding of α-syn.

This study delineates a novel mode of protein interaction for Ru(III) compounds. Since NAMI-A has low toxicity in humans, it and other complexes in this class, have potential for development as drugs for relieving the symptoms of Parkinson's and other neurodegenerative conditions.

Experimental Section

Protein Expression and Purification. The cDNA fragment encoding the full-length α-synuclein (α-syn) was obtained by gene synthesis and amplified by polymerase chain reaction (PCR). The PCR product was inserted into a pST-GB1 vector that encodes an N-terminal His_6-tag followed by a GB1-tag and a TEV cleavage site. The plasmid was transformed into BL21 (DE3) competent cells for overexpression of fusion protein. The uniformly ^{15}N isotopically-labeled protein was obtained from the growth of *E. coli* in the minimal medium containing $^{15}NH_4Cl$ as the sole nitrogen source. ^{13}C-methyl selective labeling of α-syn methionines was achieved by growing *E. coli* in a M9 medium containing $^{13}CH_3$-labeled methionine. The protein was first

purified using Ni-NTA affinity chromatography. The GB1-tag was cleaved by TEV protease, and was removed using Ni-NTA affinity chromatography. The protein was further purified through gel filtration on fast protein liquid chromatography (AKTA).

Preparation of α-syn oligomers and fibrils. Oligomeric α-syn species were prepared using the literature method.[16a, 23] Briefly, monomeric α-syn in Milli-Q water was lyophilized and subsequently resuspended in PBS (pH 7.4, contains 137 mM NaCl) at ca. 0.8 mM (12 mg/mL). The resulting solution was passed through a filter (0.22 μm cutoff) and then incubated at 37 °C for 20-24 h under quiescent conditions. The excess monomeric protein and small oligomers were removed by multiple steps of ultrafiltration (100 kDa cutoff). The final concentration of oligomers was measured based on the absorbance at 275 nm using a molar extinction coefficient of 5,600 $M^{-1}{\cdot}cm^{-1}$.

The preformed α-syn fibrils (PFFs) were prepared by incubation of 0.36 mM (5 mg/mL) α-syn monomer in PBS buffer at 37 °C in a shaker (1000 rpm). After 5 days incubation, the fibrils were collected by centrifugation (20,000 g) and resuspended in PBS buffer. The samples were stored at -80 °C. The formation of amyloid fibrils was confirmed by using thioflavin fluorimetry and TEM imaging.

***In vivo* assays.** Male Sprague-Dawley rats (200-250 g) were obtained from Department of Neurosurgery, Anhui Provincial Hospital Affiliated to University of Science and Technology of China. The animals received food and water ad libitum and were kept under strictly controlled environmental conditions (12 h light/dark cycle, with light on between 7:00 and 19:00 o'clock; room temperature 25 °C). The animal experiments were approved by the Animal Research Ethics Committee of the First Affiliated Hospital of the University of Science and Technology of China (Accreditation number: 20210719114600037291).

Rats were deeply anesthetized with chloral hydrate (300 mg/kg, i.p.) and placed in a Kopf stereotaxic apparatus (Narishige, Japan). An injection cannula was slowly inserted through a hole drilled into the skull in the central part of the left striatum of each animal using the following coordinates (in millimeters): anteroposterior 0 mm; mediolateral ±2.5 mm; dorsoventral -5.0 mm.[42] The preformed α-syn fibrils (PFFs) were injected into the left striatum, whereas the contralateral side was left intact. Infusions were performed during surgery; PFFs (10 mg/mL, equivalent to 0.7 mM in monomer) were configured in PBS and delivered at a flow rate of 0.5 μL/min for 4 min. The cannula was slowly removed after the infusion and the incision was tightly closed after 5 min.

After the injection PFFs, NAMI-A was treated on the 30th day. On the 50th day, the rats were examined for spontaneous behavioral abnormalities by apomorphine (APO)-induced rotational asymmetry assessment. The number of rotations to the ipsilateral side was counted for 30 min starting from 10 min after an intraperitoneal administration of APO (0.5 mg/kg). All the testing was done repeatedly at the 50th day after unilateral administration of PFFs. PBS-injected animals were tested at the same time points as a control. (See Supporting Information for more detailed experimental procedures.)

Acknowledgements

This work was supported by National Key R&D Program of China (2017YFA0505400, 2020YFA0710700), the National Natural Science Foundation of China (22177109, 21877103, 52021002). A portion of this work was performed on the Steady High Magnetic Field Facilities, High Magnetic Field Laboratory, CAS. P.J.S. research on Platinum Group Metals is supported by Anglo American.

Keywords: ruthenium complex • ligand substitution kinetics • protein aggregation inhibition • protein target sites • Parkinson's disease

[1] a) E. Boros, P. J. Dyson, G. Gasser, *Chem* **2020**, *6*, 41-60; b) E. J. Anthony, E. M. Bolitho, H. E. Bridgewater, O. W. L. Carter, J. M. Donnelly, C. Imberti, E. C. Lant, F. Lermyte, R. J. Needham, M. Palau, P. J. Sadler, H. Y. Shi, F. X. Wang, W. Y. Zhang, Z. J. Zhang, *Chem. Sci.* **2020**, *11,* 12888-12917.

[2] a) R. Trondl, P. Heffeter, C. R. Kowol, M. A. Jakupec, W. Berger, B. K. Keppler, *Chem. Sci.* **2014**, *5*, 2925-2932; b) S. M. Meier-Menches, C. Gerner, W. Berger, C. G. Hartinger, B. K. Keppler, *Chem. Soc. Rev.* **2018**, *47*, 909-928.

[3] J. M. Rademaker-Lakhai, D. van den Bongard, D. Pluim, J. H. Beijnen, J. H. M. Schellens, *Clin. Cancer Res.* **2004**, *10*, 3717-3727.

[4] S. Monro, K. L. Colon, H. M. Yin, J. Roque, P. Konda, S. Gujar, R. P. Thummel, L. Lilge, C. G. Cameron, S. A. McFarland, *Chem. Rev.* **2019**, *119*, 797-828.

[5] A. Merlino, *Coord. Chem. Rev.* **2016**, *326*, 111-134.

[6] E. Alessio, L. Messori, *Molecules* **2019**, *24*, 1995.

[7] A. R. Simovic, R. Masnikosa, I. Bratsos, E. Alessio, *Coord. Chem. Rev.* **2019**, *398,* 113011.

[8] S. M. Yuan, S. M. Chen, H. Wu, H. Jiang, S. H. Zheng, Q. L. Zhang, Y. Z. Liu, *Chem. Commun.* **2020**, *56*, 1397-1400.

[9] G. Livingston, J. Huntley, A. Sommerlad, D. Ames, C. Ballard, S. Banerjee, C. Brayne, A. Burns, J. Cohen-Mansfield, C. Cooper, S. G. Costafreda, A. Dias, N. Fox, L. N. Gitlin, R. Howard, H. C. Kales, M. Kivimaki, E. B. Larson, A. Ogunniyi, V. Orgeta, K. Ritchie, K. Rockwood, E. L. Sampson, Q. Samus, L. S. Schneider, G. Selbaek, L. Teri, N. Mukadam, *Lancet* **2020**, *396*, 413-446.

[10] a) B. Winner, R. Jappelli, S. K. Maji, P. A. Desplats, L. Boyer, S. Aigner, C. Hetzer, T. Loher, M. Vilar, S. Campioni, *Proc. Natl. Acad. Sci. U.S.A.* **2011**, *108*, 4194-4199; b) T. M. Dawson, V. L. Dawson, *Science* **2003**, *302*, 819-822; c) M. Bourdenx, A. Nioche, S. Dovero, M.-L. Arotcarena, S. Camus, G. Porras, M.-L. Thiolat, N. P. Rougier, A. Prigent, P. J. S. a. Aubert, *Sci. Adv.* **2020**, *6*, eaaz9165.

[11] a) E. Chung, Y. Choi, J. Park, W. Nah, J. Park, Y. Jung, J. Lee, H. Lee, S. Park, S. Hwang, S. Kim, J. Lee, D. Min, J. Jo, S. Kang, M. Jung, P. H. Lee, H. E. Ruley, D. Jo, *Sci. Adv.* **2020**, *6*, eaba1193; b) M. G. Savelieff, G. Nam, J. Kang, H. J. Lee, M. Lee, M. H. Lim, *Chem. Rev.* **2019**, *119*, 1221-1322.

[12] A. K. Buell, C. Galvagnion, R. Gaspar, E. Sparr, M. Vendruscolo, T. P. J. Knowles, S. Linse, C. M. Dobson, *Proc. Natl. Acad. Sci. U.S.A.* **2014**, *111*, 7671-7676.

[13] a) G. Fusco, S. W. Chen, P. T. F. Williamson, R. Cascella, M. Perni, J. A. Jarvis, C. Cecchi, M. Vendruscolo, F. Chiti, N. Cremades, L. M. Ying, C. M. Dobson, A. De Simone, *Science* **2017**, *358*, 1440-1443; b) R. Stok, A. Ashkenazi, *Nat. Rev. Mol. Cell Bio.* **2020**, *21*, 357-358.

[14] M. P. Muller, T. Jiang, C. Sun, M. Lihan, S. Pant, P. Mahinthichaichan, A. Trifan, E. J. C. r. Tajkhorshid, *Chem. Rev.* **2019**, *119*, 6086-6161.

[15] a) C. Galvagnion, A. K. Buell, G. Meisl, T. C. T. Michaels, M. Vendruscolo, T. P. J. Knowles, C. M. Dobson, *Nat. Chem. Biol.* **2015**, *11*, 229-234; b) L. Antonschmidt, R. Dervişoğlu, V. Sant, K. Tekwani Movellan, I. Mey, D. Riedel, C. Steinem, S. Becker, L. B. Andreas, C. Griesinger, *Sci. Adv.* **2021**, *7*, eabg2174.

[16] a) M. Perni, C. Galvagnion, A. Maltsev, G. Meisl, M. B. D. Muller, P. K. Challa, J. B. Kirkegaard, P. Flagmeier, S. I. A. Cohen, R. Cascella, S. W. Chen, R. Limboker, P. Sormanni, G. T. Heller, F. A. Aprile, N. Cremades, C. Cecchi, F. Chiti, E. A. A. Nollen, T. P. J. Knowles, M. Vendruscolo, A. Bax, M. Zasloff, C. M. Dobson, *Proc. Natl. Acad. Sci. U.S.A.* **2017**, *114*, 1009-1017; b) M. Perni, P. Flagmeier, R. Limbocker, R. Cascella, F. A. Aprile, C. Galvagnion, G. T. Heller, G. Meisl, S. W. Chen, J. R. Kumita, P. K. Challa, J. B. Kirkegaard, S. I. A. Cohen, B. Mannini, D. Barbut, E. A. A. Nollen, C. Cecchi, N. Cremades, T. P. J. Knowles, F. Chiti, M. Zasloff, M. Vendruscolo, C. M. Dobson, *Acs Chem. Biol.* **2018**, *13*, 2308-2319.

[17] a) B. A. Killinger, R. Melki, P. Brundin, J. H. Kordower, *Npj Parkinsons Dis.* **2019**, *5,* 23; b) J. Lautenschlager, A. D. Stephens, G. Fusco, F. Strohl, N. Curry, M. Zacharopoulou, C. H. Michel, R. Laine, N. Nespovitaya, M. Fantham, D. Pinotsi, W. Zago, P. Fraser, A. Tandon, P. St George-Hyslop, E. Rees, J. J. Phillips, A. De Simone, C. F. Kaminski, G. S. K. Schierle, *Nat. Commun.* **2018**, *9, 712*.

[18] a) H. Wood, *Nat. Rev. Neurol.* **2020**, *16*, 184; b) J. Brooks, J. Everett, F. Lermyte, V. T. Tjhin, P. J. Sadler, N. Telling, J. F. Collingwood, *J. Trace Elem. Med. Bio.* **2020**, *62,* 126555; c) J. Everett, F. Lermyte, J. Brooks, V. Tjendana-Tjhin, G. Plascencia-Villa, I. Hands-Portman, J. M. Donnelly, K. Billimoria, G. Perry, X. W. Zhu, P. J. Sadler, P. B. O'Connor, J. F. Collingwood, N. D. Telling, *Sci. Adv.* **2021**, *7,* eabf6707.

[19] Y. Sheng, Z. Hou, S. Cui, K. Cao, S. Yuan, M. Sun, J. Kljun, G. Huang, I. Turel, Y. Liu, *Chem. Eur. J.* **2019**, *25*, 12789-12794.

[20] J. A. Rodriguez, M. I. Ivanova, M. R. Sawaya, D. Cascio, F. E. Reyes, D. Shi, S. Sangwan, E. L. Guenther, L. M. Johnson, M. Zhang, L. Jiang, M. A. Arbing, B. L. Nannenga, J. Hattne, J. Whitelegge, A. S. Brewster, M. Messerschmidt, B. Boutet, N. K. Sauter, T. Gonen, D. S. Eisenberg, *Nature* **2015**, *525*, 486-490.

[21] G. Fusco, A. De Simone, T. Gopinath, V. Vostrikov, M. Vendruscolo, C. M. Dobson, G. Veglia, *Nat. Commun.* **2014**, *5.* 3827.

[22] a) D. R. Whiten, D. Cox, M. H. Horrocks, C. G. Taylor, S. De, P. Flagmeier, L. Tosatto, J. R. Kumita, H. Ecroyd, C. M. Dobson, D. Klenerman, M. R. Wilson, *Cell Rep.* **2018**, *23*, 3492-3500; b) E. M. Rocha, B. De Miranda, L. H. Sanders, *Neurobiol. Dis.* **2018**, *109*, 249-257.

[23] K. C. Luk, V. Kehm, J. Carroll, B. Zhang, P. O'Brien, J. Q. Trojanowski, V. M. Y. Lee, *Science* **2012**, *338*, 949-953.

[24] S. Zhang, Y. Q. Liu, C. Jia, Y. J. Lim, G. Feng, E. Xu, H. Long, Y. Kimura, Y. Tao, C. Zhao, C. Wang, Z. Liu, J. J. Hu, M. R. Ma, Z. Liu, L. Jiang, D. Li, R. Wang, V. L. Dawson, T. M. Dawson, Y. M. Li, X. Mao, C. Liu, *Proc. Natl. Acad. Sci. U.S.A.* **2021**, *118,* e2011196118.

[25] M. G. Spillantini, R. A. Crowther, R. Jakes, M. Hasegawa, M. Goedert, *Proc. Natl. Acad. Sci. U.S.A.* **1998**, *95*, 6469-6473.

[26] J. T. Bendor, T. P. Logan, R. H. Edwards, *Neuron* **2013**, *79*, 1044-1066.

[27] L. Tatenhorst, K. Eckermann, V. Dambeck, L. Fonseca-Ornelas, H. Walle, T. L. da Fonseca, J. C. Koch, S. Becker, L. Toenges, M. Bahr, T. F. Outeiro, M. Zweckstetter, P. Lingor, *Acta Neuropathol. Com.* **2016**, *4,* 39.

[28] R. Moons, A. Konijnenberg, C. Mensch, R. Van Elzen, C. Johannessen, S. Maudsley, A.-M. Lambeir, F. Sobott, *Sci. Rep.* **2020**, *10*, 16293.

[29] E. Alessio, *Eur. J. Inorg. Chem.* **2017**, 1549-1560.

[30] L. Chiniadis, P. Giastas, I. Bratsos, A. Papakyriakou, *Inorg. Chem.* **2021**, *60*, 10729-10737.

[31] J. Bieschke, J. Russ, R. P. Friedrich, D. E. Ehrnhoefer, H. Wobst, K. Neugebauer, E. E. Wanker, *Proc. Natl. Acad. Sci. U.S.A.* **2010**, *107*, 7710-7715.

[32] T. Yeung, G. E. Gilbert, J. Shi, J. Silvius, A. Kapus, S. Grinstein, *Science* **2008**, *319*, 210-213.

[33] T. Srivastava, R. Raj, A. Dubey, D. Kumar, R. K. Chaturvedi, S. K. Sharma, S. Priya, *Sci. Rep.* **2020**, *10,* 18412.

[34] A. Pineda, J. Burre, *Proc. Natl. Acad. Sci. U.S.A.* **2017**, *114*, 1223-1225.

[35] a) L. Fonseca-Ornelas, S. E. Eisbach, M. Paulat, K. Giller, C. O. Fernandez, T. F. Outeiro, S. Becker, M. Zweckstetter, *Nat. Commun.* **2014**, *5*, 5857; b) A. Mahapatra, S. Sarkar, S. C. Biswas, K. Chattopadhyay, *Chem. Commun.* **2019**, *55*, 11052-11055.

[36] M.-J. Kim, S.-B. Oh, J. Kim, K. Kim, H.-S. Ryu, M. S. Kim, S. Ayton, A. I. Bush, J.-Y. Lee, S. J. Chung, *Parkinsonism Relat. Disord.* **2018**, *55*, 117-121.

[37] H. R. Lucas, J. C. Lee, *Metallomics* **2011**, *3*, 280-283.

[38] J. C. Lee, H. B. Gray, J. R. Winkler, *J. Am. Chem. Soc.* **2008**, *130*, 6898-6899.

[39] R. M. Rasia, C. W. Bertoncini, D. Marsh, W. Hoyer, D. Cherny, M. Zweckstetter, C. Griesinger, T. M. Jovin, C. O. Fernandez, *Proc. Natl. Acad. Sci. U.S.A.* **2005**, *102*, 4294-4299.

[40] A. Bijelic, S. Theiner, B. K. Keppler, A. Rompel, *J. Med. Chem.* **2016**, *59*, 5894-5903.

[41] S. Kim, S. H. Kwon, T. I. Kam, N. Panicker, S. S. Karuppagounder, S. Lee, J. H. Lee, W. R. Kim, M. Kook, C. A. Foss, C. Shen, H. Lee, S. Kulkarni, P. J. Pasricha, G. Lee, M. G. Pomper, V. L. Dawson, T. M. Dawson, H. S. Ko, *Neuron* **2019**, *103*, 627-641.
[42] C. S. Niu, J. M. Mei, Q. Pan, X. M. Fu, *Appl. Neurophysiol.* **2009**, *87*, 69-81.